A combined wear-fatigue design methodology for fretting in the pressure armour layer of flexible marine risers

S.M. O'Halloran[a], P.H. Shipway[b], A.D. Connaire[c], S.B. Leen[a1*], A.M. Harte[d1]

[a] Mechanical Engineering, National University of Ireland, Galway, Ireland

[b] Faculty of Engineering, University of Nottingham, Nottingham, UK

[c] Wood Group Kenny, Galway Technology Park, Parkmore, Galway, Ireland

[d] Civil Engineering, National University of Ireland, Galway, Ireland

[1] Joint senior authors

* Corresponding author: Prof. Sean Leen, sean.leen@nuigalway.ie

Abstract

This paper presents a combined experimental and computational methodology for fretting wear-fatigue prediction of pressure armour wire in flexible marine risers. Fretting wear, friction and fatigue parameters of pressure armour material have been characterised experimentally. A combined fretting wear-fatigue finite element model has been developed using an adaptive meshing technique and the effect of bending-induced tangential slip has been characterised. It has been shown that a surface damage parameter combined with a multiaxial fatigue parameter can accurately predict the beneficial effect of fretting wear on fatigue predictions. This provides a computationally efficient design tool for fretting in the pressure armour layer of flexible marine risers.

Keywords: Fretting wear, fretting crack initiation, fretting life prediction, flexible risers, pressure armour wire

1 Introduction

Fretting is a form of surface damage that occurs between nominally static surfaces in contact experiencing cyclic tangential loading, resulting in a non-uniform, small-scale (typically micro- or nano-scale) relative slip. Dobromirski [1] proposed that there are up to fifty variables that affect fretting behaviour. There are three slip regimes associated with fretting [2]: (i) partial slip (PS), (ii) gross slip (GS), and, (iii) mixed slip (MS). The slip regime is dependent on loading conditions (normal and tangential loads) and the coefficient of friction (CoF) between the two surfaces [1]. Vingsbo and Söderberg [2] observed the relationship between applied slip amplitude, fatigue life and wear rate for a fretting fatigue test (Figure 1). There is little effect of wear in the stick region and, since there is little or no relative motion, high fatigue life is observed. Partial slip occurs as slip amplitude increases; wear remains low in this slip regime, but fatigue life decreases dramatically reaching a minimum value at the partial-gross slip transition. In gross slip, wear becomes the predominant damage mechanism and fatigue life increases; this has been attributed [3] to embryonic cracks being "worn away" before they nucleate to a significant length. Leen and co-workers [4] have also shown that this increase can be attributed to and predicted on the basis of the wear-induced re-distribution of contact stresses. In addition to contact load and slip amplitude, coefficient of friction and wear coefficient are key variables in this tribological process.

Fretting is a potential problem in many engineering applications such as spline couplings in aero-engine main-shafts [5 - 6], gas turbine dovetail joints [7], steel wire ropes [8 - 9], flexible marine risers [10 - 11] and other industrial applications. Flexible marine risers are a key component in the delivery of offshore hydrocarbons from the seabed to sea level, typically to a floating structure, such as a platform or vessel. In recent decades, flexible marine risers have transformed the oil and gas industry, allowing for hydrocarbon extraction

at deeper depths and higher pressures in comparison to the traditional rigid structures. The structural integrity of flexible risers is paramount to personnel and environmental safety. Also, the economic implications of riser failure are significant. Flexible risers rely on a complex, composite cross-sectional architecture of helically-wound, interlocking steel wires and polymer layers to give a unique combination of high bending flexibility, axial and torsional stiffness and internal pressure resistance, as well as internal and external corrosion resistance (see Figure 2) [12]. The research presented here focuses on the helically-wound, interlocked metallic wires, which form the pressure armour layer; the primary function of this layer is to contain internal pressure and resist hoop stress. For the inter-locking steel wires, micro-articulation of the nub and groove mechanical contacts (Figure 2) plays a key role in achieving the complex combination of exceptional mechanical properties in flexible risers. Normal forces due to internal hydrocarbon and external water pressure, as well as radial stresses from the tensile armour layer, keep the nub and groove of the pressure armour in contact. Failure of these sub-layers due to fatigue is one of the main considerations during the design phase of the flexible riser.

The effects of fretting wear and fretting fatigue on flexible risers is complex to analyse. The American Petroleum Industry (API) design codes recommend a safety factor of 10 for fatigue design of pressure armour layers [13], to account for uncertainties, including fretting, for example. In marine risers, fretting action may be caused by cyclic loads such as shearing loads due to bending or fluctuations in hydrocarbon pressure. Hence, there is a potential for micro-scale cyclic frictional contact stresses and slip leading to micro-scale surface damage, typically, a combination of wear and fatigue micro-crack nucleation, ultimately leading to loss of function and fatigue cracking and failure. The predominance of wear or fatigue crack nucleation is dependent on a large number of mechanical and physical variables; therefore the development of a combined modelling and experimental capability is

critical for a service life prediction (design) methodology. Fretting behaviour in the pressure armour layer has been identified as an aspect of riser design which requires further research [14]. Løtveit and Bjaerum [15] identified fretting of the pressure armour wire as a potential failure mode for flexible marine risers; however, this has received relatively little attention. Harte and McNamara [16 - 17] presented a three-dimensional analytical model for stress analysis of bonded flexible risers. Féret [18] presented a theoretical approach to calculate stresses, contact pressures and slip between tensile armour layers of flexible pipes under axisymmetric loading. Burke and Witz [10] presented an excellent review of the problem at an industrial conference. More recently, Perera [19] presented an experimental investigation for fretting of the pressure armour layer of unbonded flexible pipes.

In this paper, experimental testing on representative pressure armour steel is presented for identification of friction and wear parameters. Fatigue testing of the pressure armour wire material is presented. A multiaxial fatigue methodology is implemented in finite element (FE) models along with an adaptive meshing technique for wear simulation. Explicit wear-fatigue modelling is used to characterise the effect of bending-induced tangential displacement on fatigue life. Furthermore, it is shown that a fretting surface damage parameter combined with the multiaxial fatigue parameter can successfully predict the beneficial effect of wear-induced stress re-distribution on fatigue. This approach has significant advantages for flexible riser fretting fatigue design.

2 Experimental

2.1 Fretting wear tests

Due to the size and complexity of geometry of the formed (extruded) pressure armour wire (see Figure 3), it was not possible to extract fretting wear test specimens for laboratory

scale fretting tests (see Figure 4) from the wire itself. Hence, in this work EN8 steel with similar chemical composition (see Table 1) and hardness to that of the pressure armour wire material has been selected for the fretting wear tests. The hardness of the EN8 was within 10% of the measured hardness of the pressure armour material. Lemm et al. [20] showed that for equal hardness fretting pairs, varying the hardness has very little effect on the total wear volume of the specimens.

Cylinder-on-flat fretting wear tests (see Figure 4a for schematic of experimental set-up) were carried out at the University of Nottingham under loading conditions as shown in Table 2. The cylinder radius, R, was 6 mm and specimen width, W, was 10 mm (see Figure 4a). Coulomb's friction law has been used, based on an idealised fretting loop as shown in Figure 4b. Coefficient of friction (CoF) is given by the ratio of tangential force (Q^*) to the normal force (P_N). From these fretting tests, the CoF evolution with fretting cycles is measured, as presented in Figure 5. The CoF starts off at ~0.2 and increases rapidly to ~0.6, due to material transfer and adhesion during metal-on-metal contact; an additional increase is then observed due to the abrasive action during the accumulation of oxidised debris; the CoF eventually stabilises (typically) to a constant value (~0.7 to 0.8) as the abrasive action decreases due to the formation of compacted debris. Increased fretting damage was observed with increasing applied displacement and normal load.

Since it is not presently straight-forward to measure the local contact slip and local contact pressure in fretting tests, the wear coefficient has been calculated using the applied normal load and slip amplitude determined from the fretting loop (see Figure 4b). In this work, three-dimensional topography of the wear scars was measured using a Bruker Contour GT-I interferometer. The wear volume, V, was calculated as the volume of material removed from the reference surface, as described in [21]. This provided data to calculate the Archard wear coefficient using the equation:

$$\frac{V}{4\delta^* N} = kP_N \tag{1}$$

where V is the wear volume, $4\delta^* N$ is the sliding distance over N cycles (see Figure 4b), k is Archard wear coefficient and P_N is the normal load applied to the specimen. An average wear coefficient was calculated as 1.1×10^{-8} MPa^{-1}, with a standard deviation of 2.1×10^{-9} MPa^{-1}, from 6 experiments conducted on 6 mm radius cylinder-on-flat fretting specimen, with varying P_N and δ^*. This methodology for calculating the wear coefficient is more accurate than that previously used by McColl et al. [22], where an average wear coefficient was calculated using multiple wear scar profiles measured using two-dimensional profilometry. It is assumed here that the value of k we identified from cylinder-on-flat tests can be more generally applied to other geometries. The contact geometry for the pressure armour layer is closely represented by the present cylinder-on-flat, i.e. it is an incomplete contact with a similar contact radius on flat. Therefore, it is assumed here that the identified Archard wear coefficient is also applicable to this geometry.

2.2 Tensile and fatigue tests

Monotonic tensile tests have been conducted on the pressure armour material extracted from a pre-service flexible marine riser, using the NUI Galway Instron servo-hydraulic testing machine and a video extensometer. The normalised stress-strain curve from this test is presented in Figure 6.

A programme of low-cycle fatigue (LCF) tests has been conducted on pressure armour material extracted from a pre-service flexible marine riser. A modified fatigue specimen geometry, based on the ASTM E606-04 [23] standard for strain-controlled fatigue testing, has been designed to facilitate use of formed pressure armour wire, following

straightening. Strain-controlled cyclic tests were carried out using the Instron servo-hydraulic testing machine, with servo-hydraulic grips and a contact extensometer for strain feedback. Tests were conducted at strain ranges of 0.8%, 1%, 1.25% and 2%. These tests have provided Coffin-Manson constants (ε'_f and c) for the computational fatigue model (see Table 3).

Computational work in this paper focuses on crack initiation; however, experimental tests typically give total life to observable cracks. Following Sweeney et al. [24], therefore, a damage approach has been implemented for back-calculation of approximate N_i for each experimentally applied strain range. A value of 0.00798 is chosen for D_c, based on a circumferential crack with depth equal to the standard element size (10 μm) initiating at the free surface. The resulting N_i data points are shown along with experimental N_f data in Figure 7. The Coffin-Manson fits for both crack initiation and failure are also shown in Figure 7. The Coffin-Manson constants (ε'_f and c) for crack initiation are presented in Table 3.

The universal slopes method [25,26] has been used to estimate the Basquin constants (σ'_f and b) for the computational fatigue model (see Table 3). The universal slopes method, in which the slopes of the plastic and elastic lines are universalised as -0.6 and -0.12 respectively for all materials, has been widely used, [26 - 27] for example. This method gives estimated high-cycle fatigue (HCF) coefficients based on monotonic tensile test results for ultimate tensile strength. The universal slopes method has been shown to give a conservative estimate for the fatigue parameters [28]. For the universal slopes method, about 80% of the data fall within a scatter-band of a factor of 3 for both HCF and LCF for a large amount of test data obtained from experiments carried out on a range of different steels [28]; this is approximately the same scatter found for different estimation methodologies.

HCF constants from the Universal slopes method are for number of cycles to failure. The number of cycles to crack initiation was back-calculated following the approach used

previously [4,29,30]. Using the Paris equation and El-Haddad correction [31] for small crack growth, the number of cycles for a crack to propagate from 10 μm to failure was calculated. The Basquin constants (σ'_f and b) for crack initiation are presented in Table 3.

3 Computational methodology

3.1 Finite element model

Previous work by the authors has focused on fretting contact in the nub-groove contact area using an axisymmetric flexible riser model [11]. In this work, a cylinder-on-flat geometry has been used to reduce the computational time of the models. It has been shown that a cylinder-on-flat is more critical in terms of fretting fatigue life in comparison to a rounded punch-on-flat geometry [32]. In an analysis of a particular rounded punch-on-flat geometry, it was found [32] that the rounded punch-on-flat had significantly lower stresses and initial fatigue damage parameter levels, despite the very localised contact edge stress (and damage) peaks, than the cylinder-on-flat case for the same normal load and stroke. Different riser manufactures have various nub-groove geometrical designs. Here, a generalised cylinder-on-flat (approximation of the actual nub-groove geometry) two-dimensional nub-groove geometry has been simulated.

A two-dimensional, plane strain assumption has been adopted for each case. The material used is a carbon steel, with a Young's modulus of 189 GPa and a Poisson's ratio of 0.3. Individual grains are not modelled in this paper; therefore, this methodology will not capture local anisotropic effect or local crystallographic heterogeneity. Hence, scatter due to microstructural effect will not be captured [33]. The radius of the cylinder is 3 mm. A CoF of 0.75 was used, based on fretting wear tests on representative pressure armour layer material.

Since the analysis is a frictional contact problem, two-dimensional, reduced integration, 4-noded, quadrilateral, plane strain elements (CPE4) were used due to their accuracy and stability for these loading conditions [22]. A mesh sensitivity study was used to establish a converged mesh; the resulting mesh is highly refined in the contact region, becoming coarser further from the contact area (see Figure 8). The contact element size is approximately 10 μm × 10 μm. The transition between fine mesh and coarse mesh is achieved by reducing the mesh density through an unstructured mesh between the fine and coarse meshes.

The master-slave algorithm for finite sliding contact within Abaqus [34] was used to define the surface interaction for both models. The maximum allowable penetration depth between master and slave nodes was set to 1 μm. The adjustment tolerance for the initial geometry was set to 0.001 μm. Since Coulomb-Amontons' Law is assumed for sliding friction, the exact stick condition is ensured by implementing Coulomb friction based on the Lagrange multiplier contact algorithm.

The dimensions of the substrate material were made significantly larger than the contact area so that the assumption of an elastic half-space remained valid. The bottom edge of the substrate was restrained in the y direction and the left and right edges were restrained in the x direction. Normal load per unit length (P) of 50 N/mm is applied to the cylinder, and a superimposed cyclic tangential displacement (Δ^*) is applied as shown in the loading history of Figure 9.

3.2 Fatigue model

For fretting fatigue crack initiation, the stress range is a primary parameter for the calculation of fatigue life. High shear stress (τ_{xy}) ranges are generally considered to be

responsible for fatigue crack initiation, and high tangential (trailing edge) stress (σ_{xx}) ranges for Mode I fatigue crack propagation [35]. Since the contact loading is cyclic, a material point can experience a high shear stress and a low tangential stress at one instant in a cycle, and subsequently at a later instant (e.g. half-cycle later) a low shear stress and a high tangential stress; this behaviour increases the possibility of crack formation and growth due to fretting [36]. Fretting fatigue crack initiation and growth can occur under both low- and high-cycle fatigue conditions, depending inter-alia on local stresses, material strength and frictional and wear conditions.

The Smith-Watson-Topper (SWT) fatigue parameter [37] combines both the Coffin-Manson equation for low-cycle fatigue (LCF) and Basquin's equation for high-cycle fatigue (HCF), as follows:

$$SWT = \frac{\sigma_{\max} \Delta\varepsilon_a}{2} = \frac{(\sigma'_f)^2}{E}(2N_i)^{2b} + \sigma'_f \, \varepsilon'_f \, (2N_i)^{b+c} \tag{2}$$

where σ_{max} is the maximum normal stress on the critical plane (for mean stress effect), $\Delta\varepsilon_a$ is the maximum normal strain amplitude on the same plane, E is Young's modulus, σ'_f and b are fatigue strength coefficient and exponent, ε'_f and c are the fatigue ductility coefficient and exponent, and N_i is the number of cycles to crack initiation.

It has been observed that fatigue cracks initiate and grow on preferential planes within a material, where the orientation depends on the normal stresses and strains on the plane. A two-dimensional critical-plane implementation of the SWT parameter, which has previously been validated for fretting fatigue by the authors [11] based on the previous work of Leen and co-workers [4, 21], is incorporated. This is a combined stress and strain transformation (covering 360° in 5° increments) process, applied to the FE models of the pressure armour layer, to identify the critical plane value and orientation from the history of cyclic multiaxial

stresses and strains on each candidate plane. SWT was calculated at the element integration points (coincident with element centroid for CPE4R elements) for 3 rows of elements close to the surface of the substrate (flat). Equation ((2) is then solved numerically using a Newton-Raphson solution scheme to predict the number of fretting cycles to crack nucleation. Sum et al. [38] showed that mesh refinement and a critical plane approach can capture stress gradient effects, associated with different contact cylinder-on-flat sizes [39 - 40], similar to the volume averaging method used by other researchers [41]. This has been attributed to the inbuilt averaging of stresses and strains over FE reduced integration elements during FE analysis [38]. This methodology of Sum et al. [38] was implemented in this work.

3.3 Wear model

The wear model utilised here is an adaptive mesh methodology, which has been implemented in Abaqus via the UMESHMOTION user sub-routine to simulate the fretting wear process and based on the modified Archard wear equation proposed by McColl et al. [22]. The fretting wear depth is calculated by applying Archard's equation to the local contact conditions along the contact area. The local wear depth is given by [4]:

$$\Delta h(x,t) = k_l\, p(x,t)\delta(x,t) \tag{3}$$

where $\Delta h(x, t)$, $p(x, t)$ and $\delta(x, t)$ are the incremental wear depth, contact pressure and relative slip at a point x on the contact surface at time t and k_l is the local wear coefficient. McColl et al. [22] describes how the FE simulation of wear requires a local wear coefficient, k_l, which is expressed as the wear per unit local slip per unit local contact pressure. However, this is wear coefficient, k, per unit displacement per unit load (as described earlier in Section 2.1). It

has been shown [22,42] that there is a close relationship between the local wear coefficient k_l and the experimentally determined volumetric wear coefficient *k*.

To reduce the computational time for fretting wear simulations, a cycle jumping technique [22,43] was employed, where it is assumed that the contact pressure and slip distributions remain constant over ΔN cycles. Therefore Equation ((3) becomes:

$$\Delta h(x,t) = \Delta N k_l \, p(x,t)\delta(x,t) \tag{4}$$

The implementation of this wear simulation algorithm in Abaqus is represented in the flowchart of Figure 10 and the adaptive meshing technique is depicted in Figure 11.

3.4 Combined wear-fatigue model

Due to the evolving geometry and stress fields associated with fretting wear, a fatigue damage accumulation model is required for prediction of fretting fatigue life. The Miner-Palmgren rule is used to calculate the damage accumulation, as follows:

$$D = \sum_{i=1}^{N} \frac{\Delta n_i}{N_i} \tag{5}$$

where Δn_i is the number of cycles experienced at loading cycle *i* with an associated SWT value of SWT_i, and N_i is the predicted number of cycles to crack initiation for SWT_i (given by Equation ((2). When D = 1, a crack is assumed to have initiated at the SWT-predicted location, orientation and number of cycles. Within the present FE methodology, D is calculated at the location of the centroid of the first row of surface elements in the unmodified mesh (prior to wear taking place).

As discussed in detail by Zhang et al. [44], in the adaptive meshing technique in the FE simulation, the centroidal position (same as Gauss point position for CPE4R elements) of each surface element changes from cycle to cycle, due to material removal and therefore damage cannot be accumulated at the same centroidal position from cycle to cycle (see Figure 11). Hence, following Zhang et al. [44], a material point mesh (MPM) has been defined, independent of the FE mesh, to calculate the damage accumulation. In this method the MPM has fixed coordinates; the SWT damage is calculated at the centroid of each element and linearly interpolated back to the MPM for calculation of accumulated damage. The spacing for the MPM is determined from the initial location of each element centroid for the unmodified mesh, following [26].

4 Results and discussion

4.1 Model validation

The SWT fatigue model used was previously [11] validated against experimental results [3] for the partial slip regime. The fretting wear model implemented has also been validated against experimental wear scar profiles. In the FE model, the cycle jump used is 1,000 cycles with 100 increments in one tangential fretting cycle; this is based on the work of Zhang et al. [32]. In

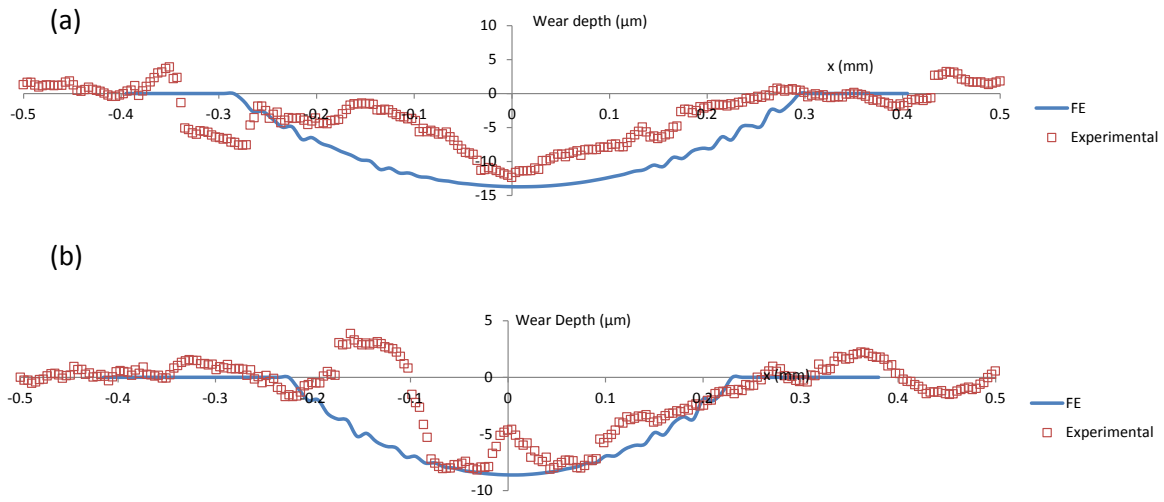

Figure 12 a comparison is made between the finite element simulated wear scars and experimentally measured fretting wear scars for R = 6 mm under two different loading conditions: (a) P_N = 500 N, Δ^* = 30 µm; and (b) P_N = 250 N, Δ^* = 15 µm. These loading conditions give a range of contact pressures and relative slips that are representative of those in the nub-groove contact of the pressure armour layer. There is a reasonable correlation between the FE simulated wear scar and the experimentally measured wear scar. The wear depth predicted by the FE model is over-predicted by 11 % (in

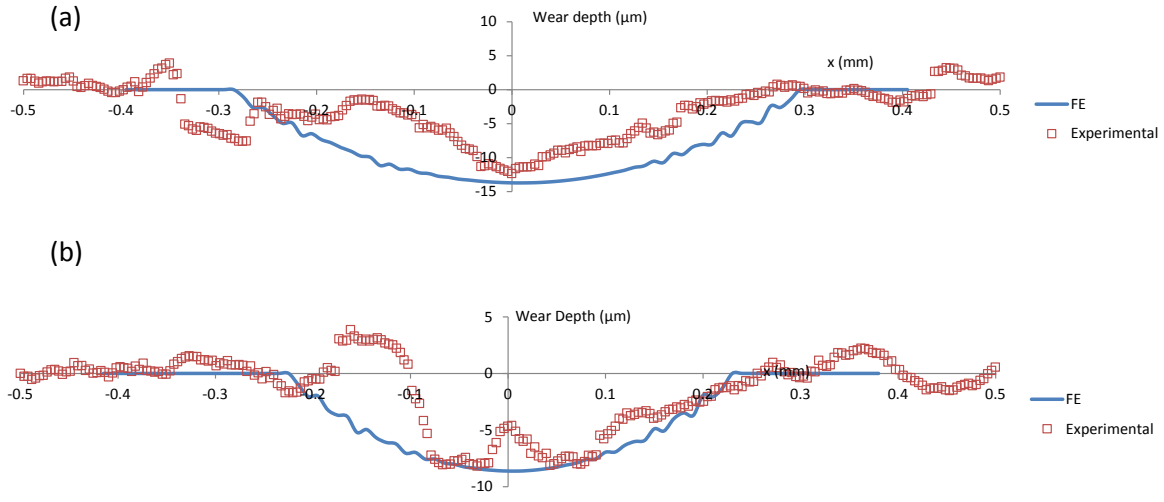

Figure 12a) and 13 % (in

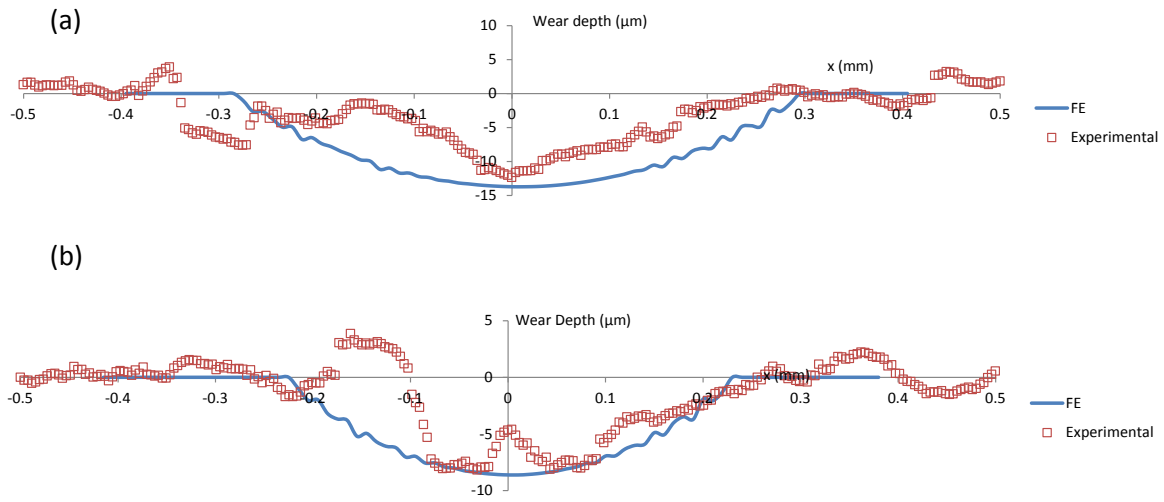

Figure 12b) in comparison to the measured experimental values. The width of the wear scar is under-predicted by 6 % in

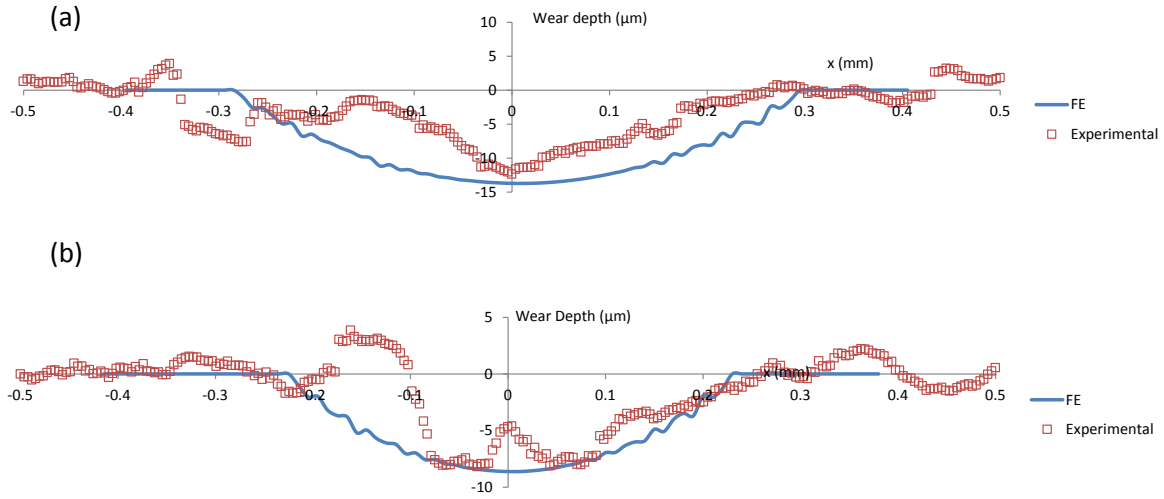

Figure 12a, and over-predicted by 24 % in

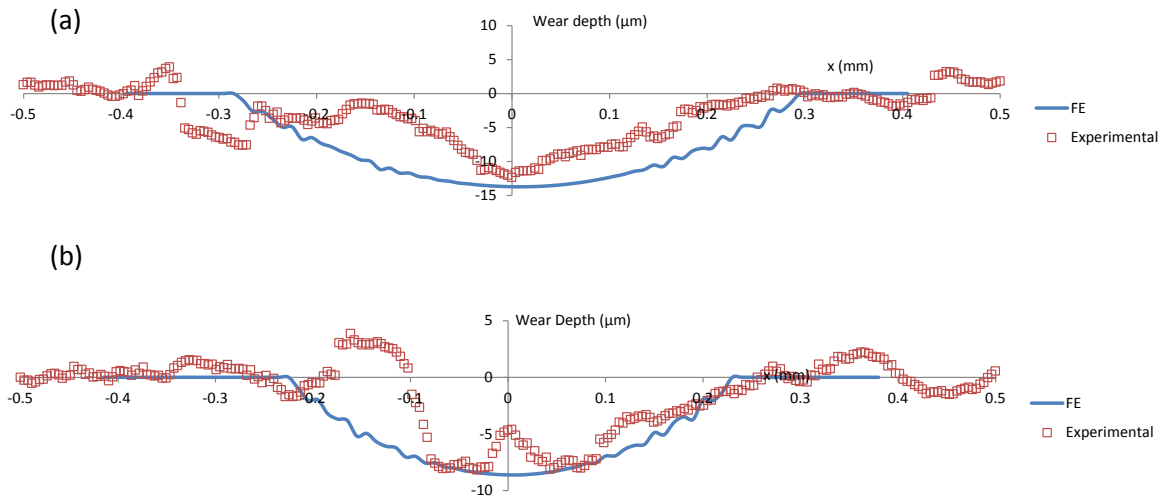

Figure 12b. In this study, as a simplification, wear of the indenter and the effects of debris are not explicitly simulated. Therefore, the effect of debris "*pile-up*", for example, as is evident in the experimental wear scar shown in

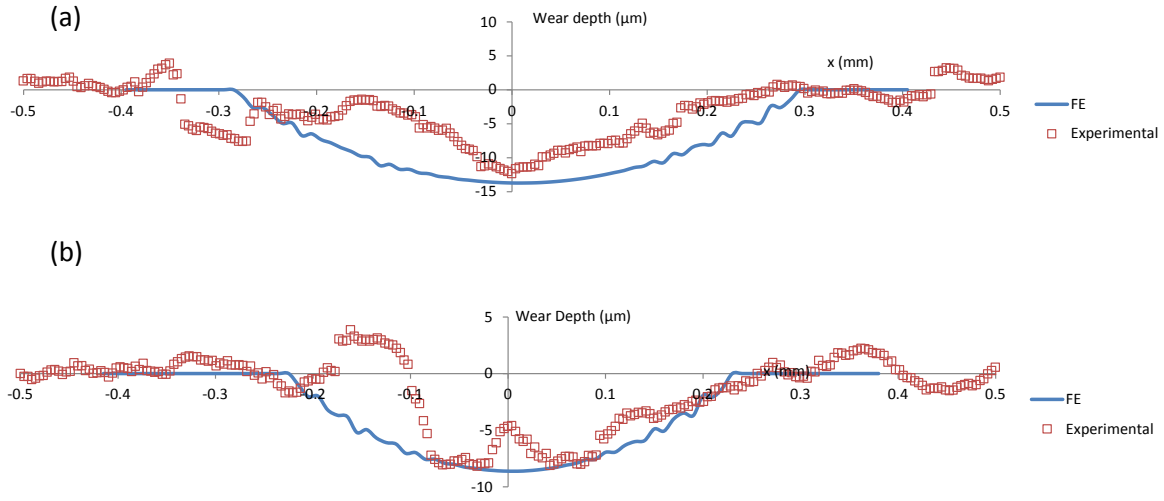

Figure 12b, is not captured in the FE wear simulation.

4.2 Effect of wear on stresses

Figure 13 presents the evolution of wear with fretting cycles for a 3 mm cylinder-on-flat model under normal load (P) of 50 N/mm and displacement amplitude (Δ^*) of 10 µm;

These loading conditions give gross slip conditions, and therefore, wear is the dominant fretting damage. Figure 14 presents the corresponding contact pressure for the 1st, 25,000th, 100,000th and 200,000th cycles. It can be seen that, as wear evolves, the contact width widens and the contact pressure is redistributed over a wider area; therefore, the peak pressure is dramatically reduced and the pressure is much less concentrated than for the initial fretting loading.

The effect of the redistribution of contact pressure on (a) tensile (σ_{xx}) and (b) shear (τ_{xy}) stresses is presented in Figure 15 for the extreme stroke position (e.g. A in loading history of Figure 9). The contact width is increased from 100 to 360 μm over 2×10^5 fretting cycles. This causes a 55 % decrease in trailing edge tensile stress value. The location of the maximum (trailing edge) tensile stress moves outwards as the contact width increases. The maximum shear stress value is initially located in the centre of contact; however, as the contact width increases, the shear stress is redistributed to an almost uniform value across the contact, which is dramatically reduced relative to the unworn case (about 75 % less that the initial peak value).

4.3 Crack Initiation

Fretting crack initiation life predictions have been calculated for element centroidal (integration point) positions at a depth of 5 μm below the surface of the substrate. When a damage of 1 is predicted for an integration point close to the surface, the element is deemed to have cracked so that initiation crack length is 10 μm. This work focuses on the interaction and competition between fatigue crack initiation (damage) and wear-induced material removal, potentially leading to either exacerbated initiation conditions (partial slip) or

ameliorated conditions (gross slip). Crack propagation is not explicitly considered in this work.

Figure 16 presents the predicted effect of applied displacement on crack initiation life with and without the effects of wear-induced material removal. In the partial and mixed slip regimes (Δ < 4 μm), the predicted crack initiation life is essentially the same for both models. However, in the gross slip regime, exclusion of wear effects is seen to significantly under-predict life. Including wear effects leads to a dramatic increase in life (to almost 10^8 cycles) with increasing stroke/displacement, relative to the minimum value in the partial slip regime. In all cases, the fretting fatigue cracks are predicted to initiate at the edge of contact. The predicted critical plane angle for crack initiation is between 10° and 30° to the x-axis (see Figure 8 for x-axis definition).

The predicted increase in fretting crack initiation life, when fretting wear is included, is attributed to the redistribution of stresses, due to the widening of the contact width and evolution of the contact geometry. This trend is consistent with the fretting schematic of Vingsbo and Söderberg [2] (Figure 1), where, as wear rate increases, the predicted fretting fatigue life increases. Hence, for flexible marine riser design, fretting wear is an important consideration in gross slip fretting analysis of the nub-groove contact, to avoid overly conservative prediction of fretting crack initiation.

4.4 Fretting design parameter including the effect of wear

The computational time for simulating fretting wear in a full or partial flexible marine riser, with multiple three-dimensional nub-groove contacts, under realistic loading histories, is prohibitively expensive for design purposes. Hence, it is proposed to adopt the D_{fret} fretting parameter, as proposed by Ding et al. [45]. The D_{fret} method introduces a surface damage

factor for the effects of fretting wear to a modified SWT approach, developed to incorporate the effects of slip and surface wear damage on crack initiation, as follows:

$$\sigma_{\max}\Delta\varepsilon_a D_{fret} = \frac{(\sigma'_f)^2}{E}(2N_i)^{2b} + \sigma'_f\,\varepsilon'_f\,(2N_i)^{b+c} \tag{6}$$

where D_{fret} is a surface damage factor given by [45]:

$$D_{fret} = (1 - C\tau\delta)\left\langle 1 - \frac{\tau\delta}{(\tau\delta)_{th}}\right\rangle^m \tag{7}$$

where C, m, and $(\tau\delta)_{th}$ are material constants; τ and δ are the local contact shear and slip, respectively. $(\tau\delta)_{\text{th}}$ has been estimated here as a value slightly greater than the value at the partial slip -gross slip transition, based on FE simulations and following Ding et al. [45]. For $\tau\delta < (\tau\delta)_{\text{th}}$, the unmodified SWT value is used (i.e. $D_{\text{fret}} = 1$); for $\tau\delta > (\tau\delta)_{\text{th}}$, the SWT-$D_{\text{fret}}$ value is used (Equation (6)).

The material constants C and m were identified by applying a least squares minimisation method to the following objective function:

$$F(C,m) = \sum_i \left\{SWT_{D,i}(C,m) - SWT_{AM,i}\right\}^2 \tag{8}$$

where $SWT_{D,i}(C,m)$ is the D_{fret} predicted SWT value at sample (element centroid) point i, $SWT_{AM,i}$ is the corresponding wear-simulated SWT value (using the adaptive meshing technique). The material constants identified for the pressure armour layer are presented in

Table 4. A comparison of wear-simulated $SWT_{\max}$ and the corresponding maximum SWT-D_{fret} value, (from the least squares minimisation method) is shown in Figure 17.

A comparison between the fretting crack initiation lives calculated using wear simulation analysis and the modified SWT-D_{fret} parameter is presented in Figure 18. This shows excellent correlation between the two prediction methods, particularly in terms of the beneficial effect of increasing (gross) slip amplitude. The major advantage of the modified SWT parameter over explicit modelling of wear is the significant reduction in computational expense.

5 Conclusion

- Tensile and fatigue tests of the pressure armour layer material from a pre-service flexible marine riser have been conducted for characterisation of mechanical behaviour. Fretting wear tests have been carried out under representative loading conditions on a representative steel with essentially the same chemical composition and hardness as pressure armour layer material. These tests have characterised the tribological behaviour of the nub-groove contact in the pressure armour layer.
- A finite element model of a cylinder-on-flat geometry, that is representative of nub-groove frictional contact, has been developed. A computational methodology, combining fretting wear simulation using adaptive meshing techniques and critical plane multiaxial fatigue life predictions, has been developed. The fretting wear finite element simulations have been validated against cylinder-on-flat fretting wear experimental test results.
- The effect of tangential displacement on fretting crack initiation life has been investigated. In partial slip, wear rate is low and therefore the detrimental effect of increasing slip on number of cycles to crack initiation is observed. However, in gross

slip wear has a beneficial effect on predicted fretting crack initiation life due to the re-distribution of stresses associated with material removal caused by wear.

- A combined surface damage and multiaxial fatigue parameter has been shown to successfully predict the effect of wear and tangential displacement on predicted fretting crack initiation life. The major benefit of this parameter is the reduced computational expense since wear does not have to be explicitly modelled. This is a key development in terms of the design of flexible risers against fretting.

Acknowledgements

The authors would like to thank the Irish Research Council and Wood Group Kenny for funding of this project through the Enterprise Partnership Scheme (EPSPG/2013/638), and the National University of Ireland for funding through an NUI Travelling Scholarship. We also wish to acknowledge the help and support we have received from Mr. Kieran Kavanagh (Wood Group Kenny), the NUI Galway Engineering Building technical staff; particularly Mr. Bonaventure Kennedy and Mr. Patrick Kelly and the Faculty of Engineering at the University of Nottingham.

References

[1] Dobromirski JM. Variables in the Fretting Process: are There 50 of Them? Standardisation of Fretting Fatigue Test Methods and Equipment. ASTM: 1992. doi:10.1520/STP25816S.

[2] Vingsbo O, Söderberg S. On fretting maps. Wear 1988;126:131–47. doi:10.1016/0043-1648(88)90134-2.

[3] Jin O, Mall S. Effects of slip on fretting behavior: experiments and analyses. Wear 2004;256:671–84. doi:10.1016/s0043-1648(03)00510-6.

[4] Madge J, Leen S, Shipway P. A combined wear and crack nucleation–propagation methodology for fretting fatigue prediction. Int J Fatigue 2008;30:1509–28. doi:10.1016/j.ijfatigue.2008.01.002.

[5] Ding J, Sum WS, Sabesan R, Leen SB, McColl IR, Williams EJ. Fretting fatigue predictions in a complex coupling. Int J Fatigue 2007;29:1229–44. doi:10.1016/j.ijfatigue.2006.10.017.

[6] Wavish PM, Houghton D, Ding J, Leen SB, Williams EJ, McColl IR. A multiaxial fretting fatigue test for spline coupling contact. Fatigue Fract Eng Mater Struct 2009;32:325–45. doi:10.1111/j.1460-2695.2009.01334.x.

[7] Ruiz C, Boddington PHB, Chen KC. An investigation of fatigue and fretting in a dovetail joint. Exp Mech 1984;24:208–17. doi:10.1007/BF02323167.

[8] Cruzado A, Hartelt M, Wäsche R, Urchegui MA, Gómez X. Fretting wear of thin steel wires. Part 1: Influence of contact pressure. Wear 2010;268:1409–16. doi:http://dx.doi.org/10.1016/j.wear.2010.02.017.

[9] Cruzado A, Hartelt M, Wäsche R, Urchegui MA, Gómez X. Fretting wear of thin steel wires. Part 2: Influence of crossing angle. Wear 2011;273:60–9. doi:http://dx.doi.org/10.1016/j.wear.2011.04.012.

[10] Burke RN, Witz JA. Fretting fatigue of flexible pipe pressure armour. Proc. Third Eur. Conf. Flex. Pipes, Unbilicals Mar. Cables - Mater. Util. Cycl. Therm. Load., Bentham Press; 1995.

[11] O'Halloran SM, Connaire AD, Harte AM, Leen SB. Modelling of fretting in the pressure armour layer of flexible marine risers. Tribol Int 2016;100:306–16. doi:10.1016/j.triboint.2016.02.040.

[12] O'Sullivan M. Meeting the future challenges of flexible pipe technology - advances in industry standards. Proc. Offshore Technol. Conf., Houston, Texas, USA: 2009.

[13] API. Recomended Practices for Flexible Marine Risers, 17J. Am Pet Ind 2009.

[14] Lange H, Berge S, Rogne T, Glomstaker T. Robust material selection in the offshore industry - flexible risers. MARINTEK, SINTEF Materials and Chemistry; 2004.

[15] Lotveit SA, Bjaerum R. Second Generation Analysis Tool for Flexible Pipes. Proc. Second Eur. Conf. Flex. Pipes, Umbilicals Mar. Cables-Structural Mech. Test., Bentham, London; 1994.

[16] McNamara JF, Harte AM. Three-dimensional analytical simulation of flexible pipe wall structure. J Offshore Mech Artic Eng 1992;114:69–75.

[17] Harte AM, McNamara JF. Modeling porcedured for stress analysis of flexible pipe cross sections. J Offshore Mech Artic Eng 1993;115:46–51.

[18] Féret JJ, Bournazel CL. Calculation of stresses and slip in structural layers of unbonded flexible pipes. J Offshore Mech Arct Eng 1987;109:263–9. doi:10.1115/1.3257019.

[19] Perera SDR, Ferando UP, Sheldrake T, Clements R. An investigation into fretting behaviour in pressure armour wires of unbonded flexible pipes. Proc. 26th Int. Conf. Offshore Mech. Arct. Eng., San Diego, California, USA: 2007.

[20] Lemm JD, Warmuth AR, Pearson SR, Shipway PH. The influence of surface hardness on the fretting wear of steel pairs—Its role in debris retention in the contact. Tribol Int 2015;81:258–66. doi:10.1016/j.triboint.2014.09.003.
[21] Warmuth AR, Shipway PH, Sun W. Fretting wear mapping: the influence of contact geometry and frequency on debris formation and ejection for a steel-on-steel pair. Proc R Soc A Math Phys Eng Sci 2015;471:20140291–20140291. doi:10.1098/rspa.2014.0291.
[22] McColl IR, Ding J, Leen SB. Finite element simulation and experimental validation of fretting wear. Wear 2004;256:1114–27. doi:10.1016/j.wear.2003.07.001.
[23] ASTM International. ASTM E606-04 Standard Practice for Strain-Controlled Fatigue Testing 2005.
[24] Sweeney CA, O'Brien B, McHugh PE, Leen SB. Experimental characterisation for micromechanical modelling of CoCr stent fatigue. Biomaterials 2014;35:36–48. doi:http://dx.doi.org/10.1016/j.biomaterials.2013.09.087.
[25] Manson SS. Fatigue: A complex subject—Some simple approximations. Exp Mech 1965;5:193–226. doi:10.1007/BF02321056.
[26] Cruzado A, Leen SB, Urchegui MA, Gómez X. Finite element simulation of fretting wear and fatigue in thin steel wires. Int J Fatigue 2013;55:7–21. doi:http://dx.doi.org/10.1016/j.ijfatigue.2013.04.025.
[27] Llano-Vizcaya L Del, Rubio-González C, Mesmacque G, Cervantes-Hernández T. Multiaxial fatigue and failure analysis of helical compression springs. Eng Fail Anal 2006;13:1303–1313. doi:10.1016/j.engfailanal.2005.10.011.
[28] Park J-H, Song J-H. Detailed evaluation of methods for estimation of fatigue properties. Int J Fatigue 1994;14:365–73.
[29] Houghton D, Wavish PM, Williams EJ, Leen SB. Multiaxial fretting fatigue testing and prediction for splined couplings. Int J Fatigue 2009;31:1805–15. doi:http://dx.doi.org/10.1016/j.ijfatigue.2008.12.005.
[30] McCarthy OJ, McGarry JP, Leen SB. Microstructure-sensitive prediction and experimental validation of fretting fatigue. Wear 2013;305:100–14. doi:10.1016/j.wear.2013.05.012.
[31] El Haddad MH, Topper TH, Smith KN. Prediction of non propagating cracks. Eng Fract Mech 1979;11:573–84. doi:10.1016/0013-7944(79)90081-X.
[32] Zhang T, McHugh PE, Leen SB. Computational study on the effect of contact geometry on fretting behaviour. Wear 2011;271:1462–80. doi:http://dx.doi.org/10.1016/j.wear.2010.11.017.
[33] McCarthy OJ, McGarry JP, Leen SB. The effect of grain orientation on fretting fatigue plasticity and life prediction. Tribol Int 2014;76:100–15. doi:http://dx.doi.org/10.1016/j.triboint.2013.09.023.
[34] DS Simulia. Abaqus 6.13 CAE User Manual 2013. http://129.97.46.200:2080/v6.13/.
[35] Hills DA, Nowell D. Mechanics of fretting fatigue. Dordrecht/Boston/London: Kluwer Academic Publishers; 1994.
[36] Szolwinski MP, Farris TN. Mechanics of fretting fatigue crack formation. Wear 1996;198:93–107. doi:10.1016/0043-1648(96)06937-2.
[37] Smith KN, Watson P, Topper TH. Stress-strain function for fatigue of metals. J Mater 1970;5:767–78.
[38] Sum W, Williams E, Leen S. Finite element, critical-plane, fatigue life prediction of simple and complex contact configurations. Int J Fatigue 2005;27:403–16. doi:10.1016/j.ijfatigue.2004.08.001.
[39] Araújo J, Nowell D. The effect of rapidly varying contact stress fields on fretting fatigue. Int J Fatigue 2002;24:763–75. doi:10.1016/S0142-1123(01)00191-8.

[40] Araújo JA, Nowell D, Vivacqua RC. The use of multiaxial fatigue models to predict fretting fatigue life of components subjected to different contact stress fields. Fatigue Fract Eng Mater Struct 2004;27:967–78. doi:10.1111/j.1460-2695.2004.00820.x.
[41] Araújo J. Analysis of pad size effects in fretting fatigue using short crack arrest methodologies. Int J Fatigue 1999;21:947–56. doi:10.1016/S0142-1123(99)00077-8.
[42] Paulin C, Fouvry S, Meunier C. Finite element modelling of fretting wear surface evolution: Application to a Ti–6A1–4V contact. Wear 2008;264:26–36. doi:10.1016/j.wear.2007.01.037.
[43] Mary C, Fouvry S. Numerical prediction of fretting contact durability using energy wear approach: Optimisation of finite-element model. Wear 2007;263:444–50. doi:10.1016/j.wear.2007.01.116.
[44] Zhang T, Harrison NM, McDonnell PF, McHugh PE, Leen SB. Micro-macro wear-fatigue of modular hip implant taper-lock coupling. J Strain Anal Eng Des 2013;49:2–18. doi:10.1177/0309324713502175.
[45] Ding J, Houghton D, Williams EJ, Leen SB. Simple parameters to predict effect of surface damage on fretting fatigue. Int J Fatigue 2011;33:332–42. doi:10.1016/j.ijfatigue.2010.09.008.

Figures

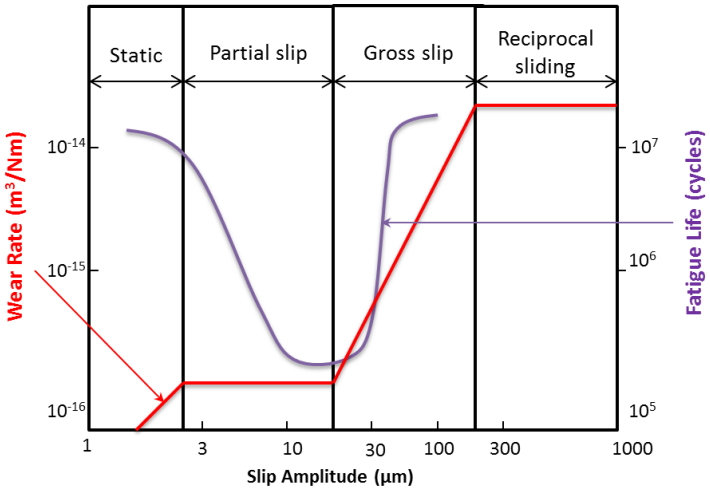

Figure 1. Schematic fretting map shows the effect of slip regime on fatigue life and wear rate (adapted from [2]).

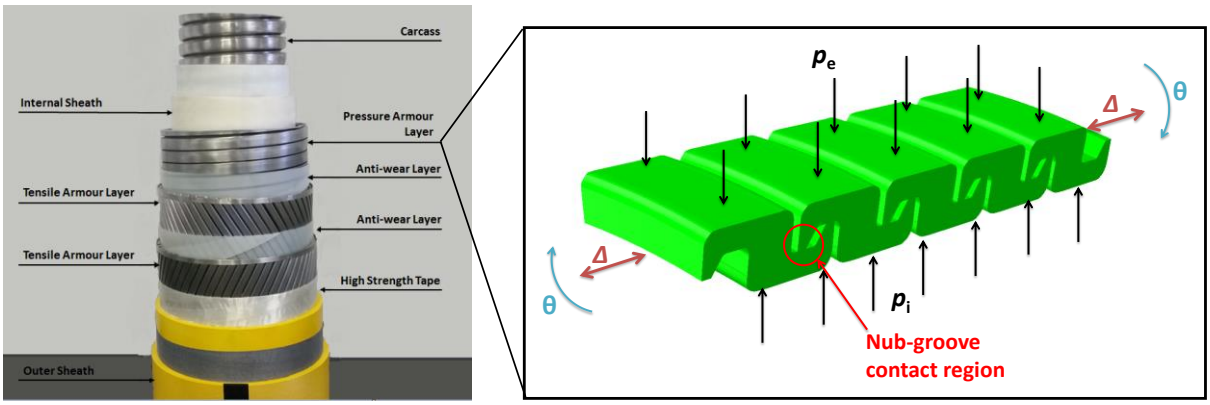

Figure 2. Photograph of a flexible marine riser cross section; loading conditions on pressure armour layer, where p_e - external pressure on risers, p_i - internal pressure on the riser, Δ - axial displacement of the pressure armour layer, θ - rotational displacement of the pressure armour layer.

(a) (b)

Figure 3. (a) Helically wound pressure armour wire in the dissected riser, and (b) pressure armour layer material extracted from the pipe

(a) (b)

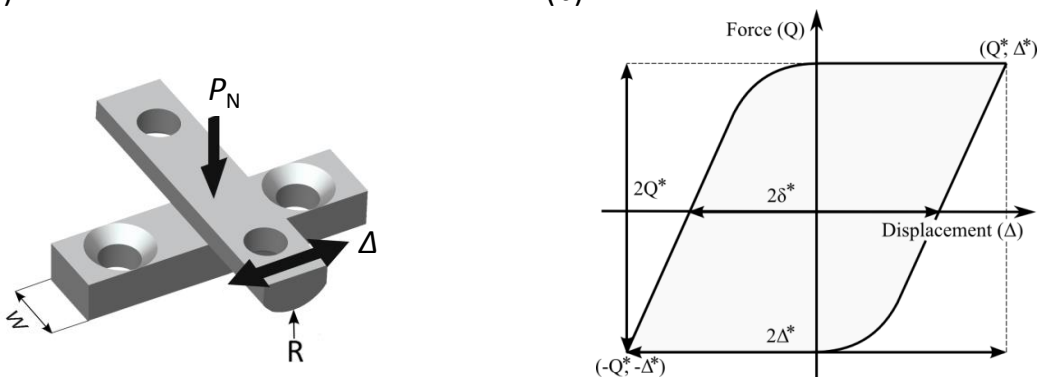

Figure 4. (a) Cylinder on flat specimen configuration used for fretting wear tests; (b) schematic diagram of an ideal fretting loop in the gross sliding regime, illustrating parameters defined in the text.

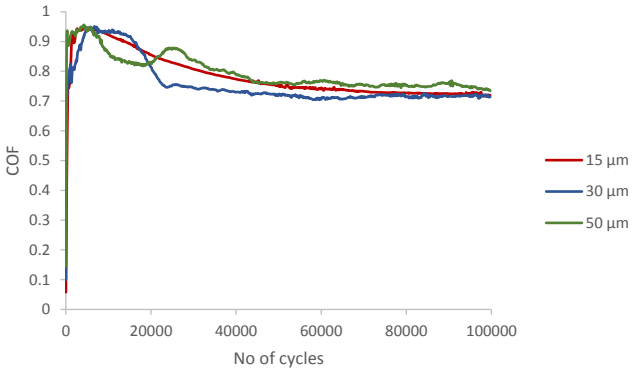

Figure 5. CoF evolution with number of fretting cycles for a pressure armour layer representative material under normal load, P_N = 250 N and applied tangential displacements, Δ = 15, 30, 50 µm.

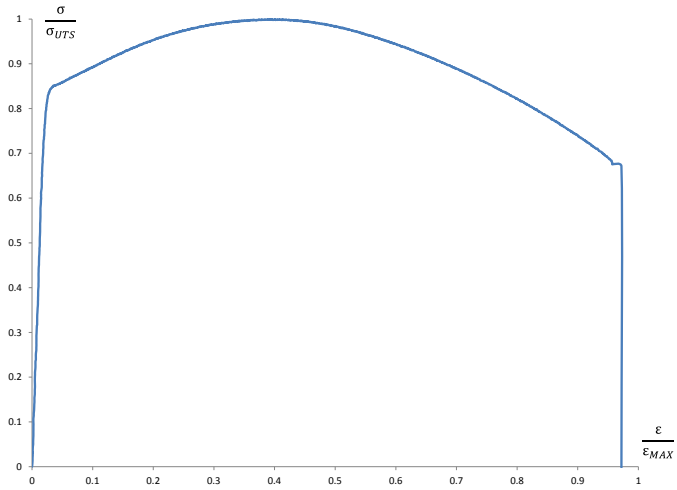

Figure 6. Normalised monotonic tensile test stress-strain curve for pressure armour material.

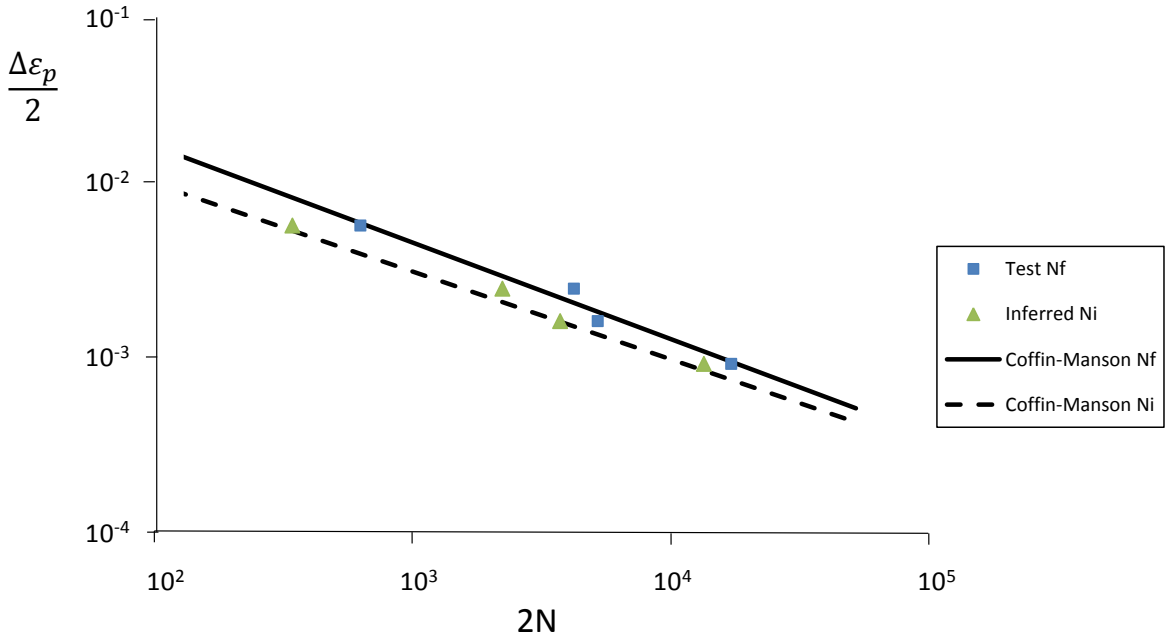

Figure 7. LCF experimental test results with Coffin-Manson fit for crack initiation and failure.

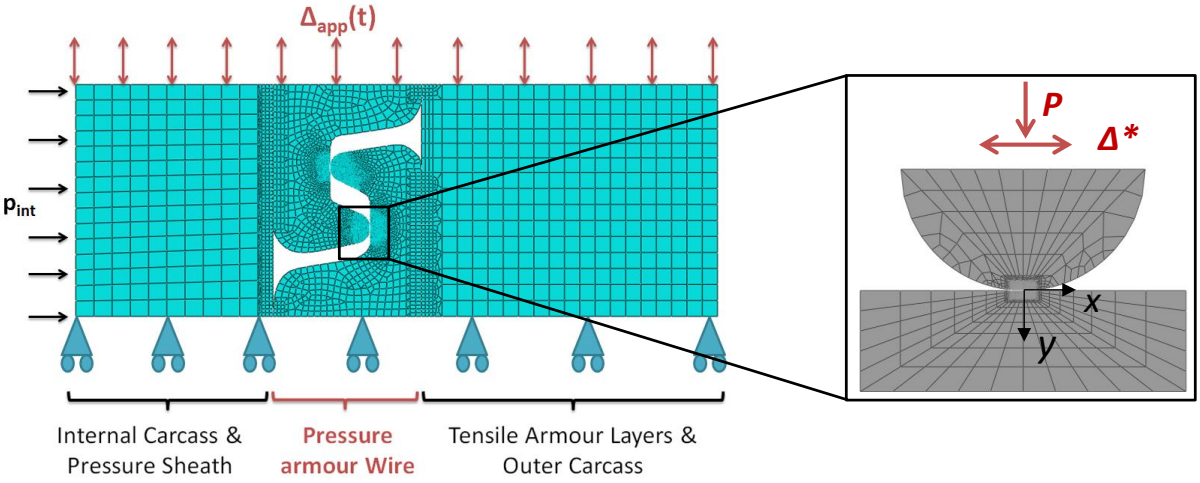

Figure 8. Axisymmetric local pressure armour model with a cylinder-on-flat nub groove geometry.

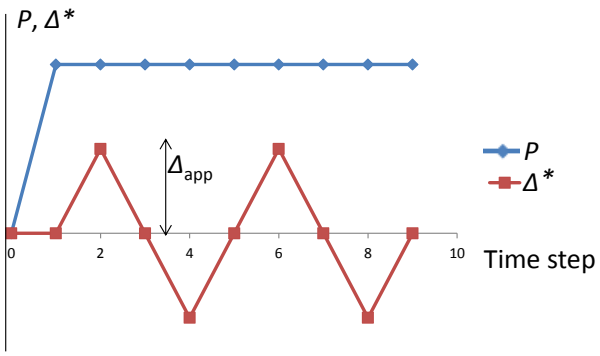

Figure 9. Applied stroke and loading history

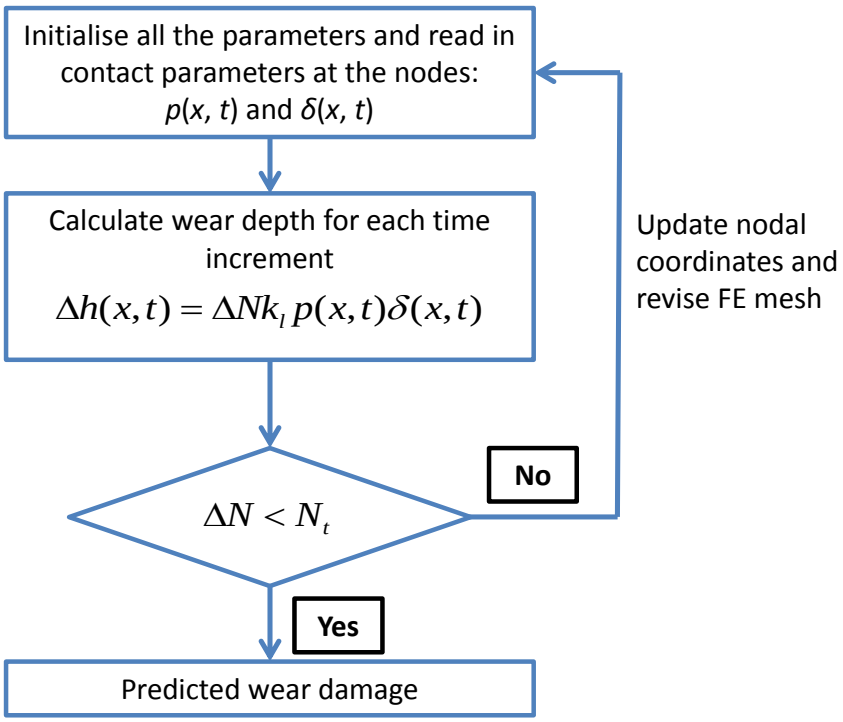

Figure 10. Methodology for implementation of the adaptive meshing technique to predict fretting wear damage.

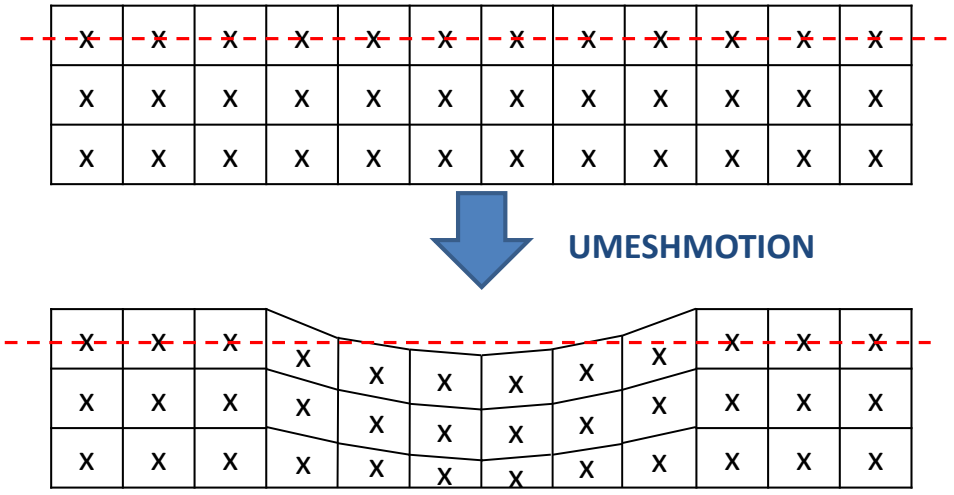

Figure 11. Finite element mesh as wear takes place for the adaptive meshing methodology [26].

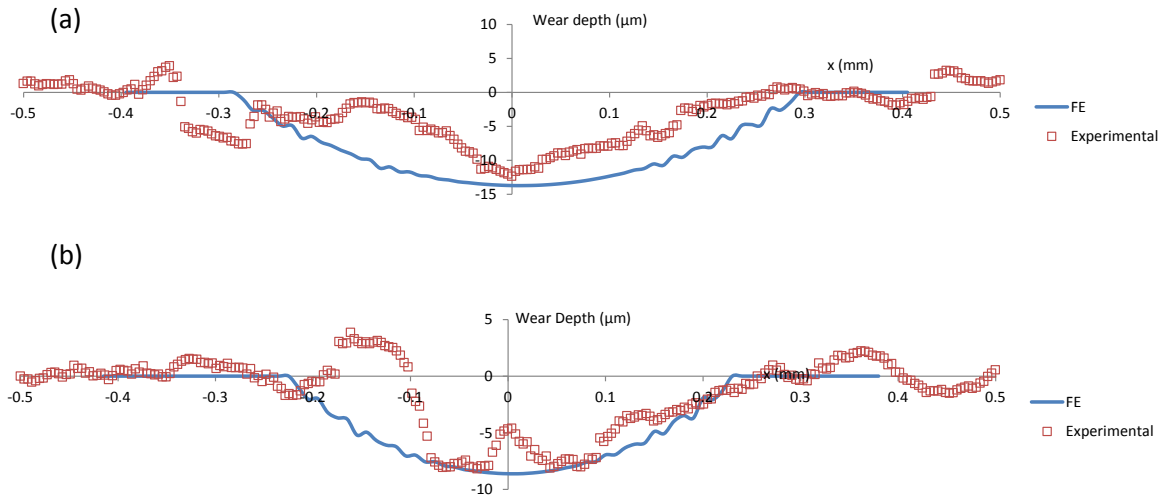

Figure 12. Comparison between finite element simulated wear scars and experimentally produced fretting wear scars for R = 6 mm after 10^5 cycles at 20 Hz and: (a) P_N = 500 N, Δ^* = 30 µm; and (b) P_N = 250 N, Δ^* = 15 µm.

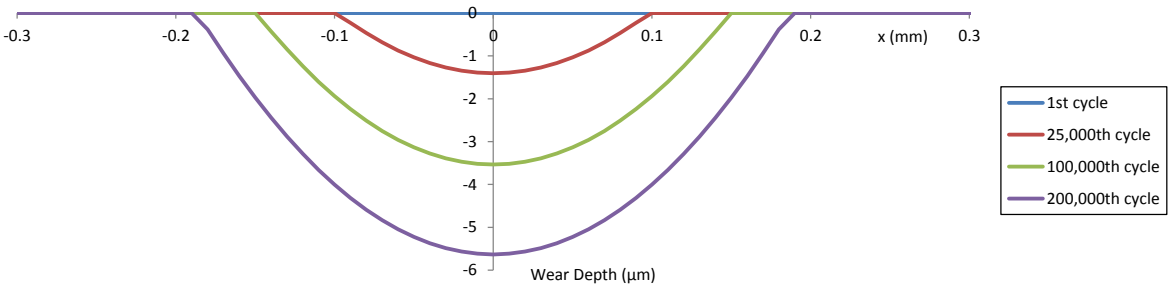

Figure 13. FE wear simulation results for gross slip (P = 50 N/mm and Δ^* = 10 μm) condition showing evolution of wear scar.

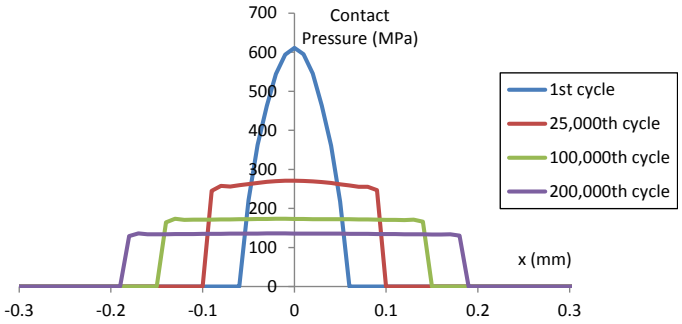

Figure 14. FE wear simulation results for gross slip (P = 50 N/mm and Δ^* = 10 μm) condition showing evolution of contact pressure.

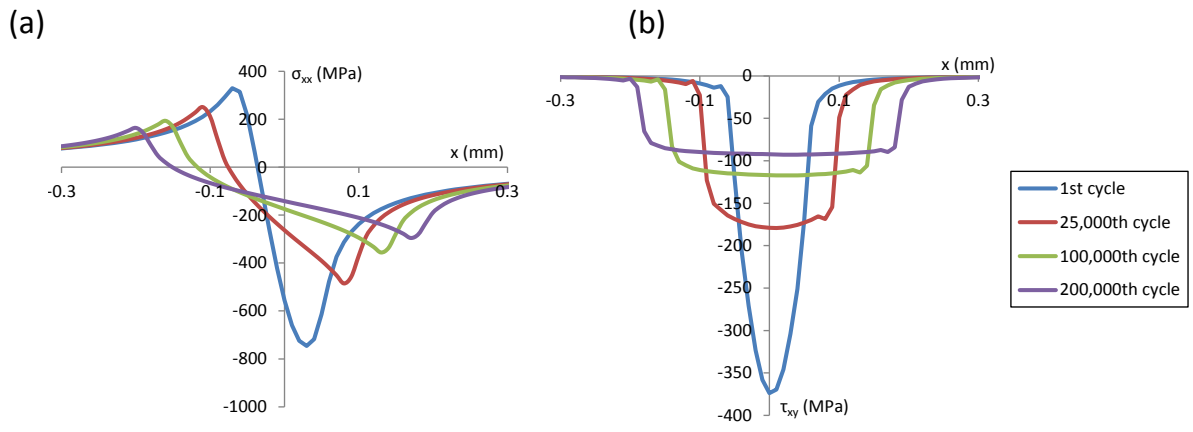

Figure 15. FE wear simulation results for gross slip (P = 50 N/mm and Δ^* = 10 μm) condition showing evolution of (a) tensile stress (σ_{xx}) and (b) shear stress (τ_{xy}) at extreme stroke position, A in Figure 9 loading history.

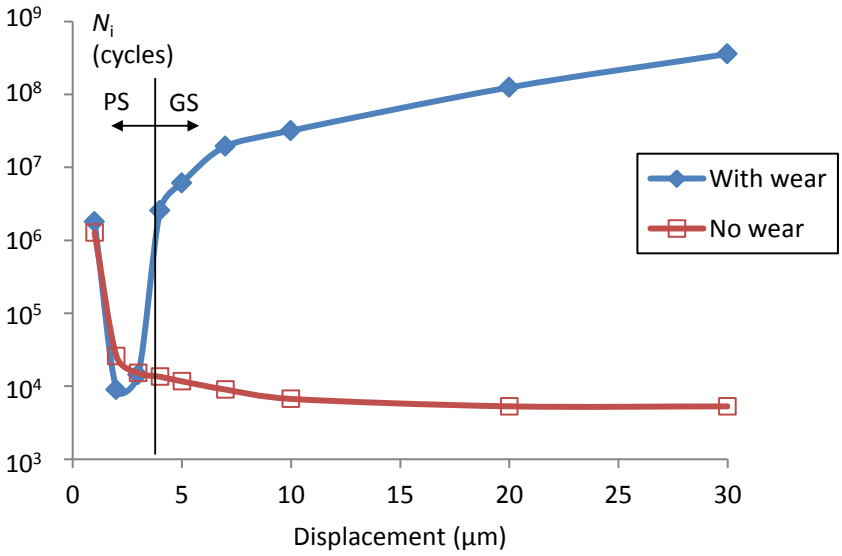

Figure 16. Predicted effect of applied tangential displacement on crack initiation life: (i) without effect of wear, and (ii) with effect of wear.

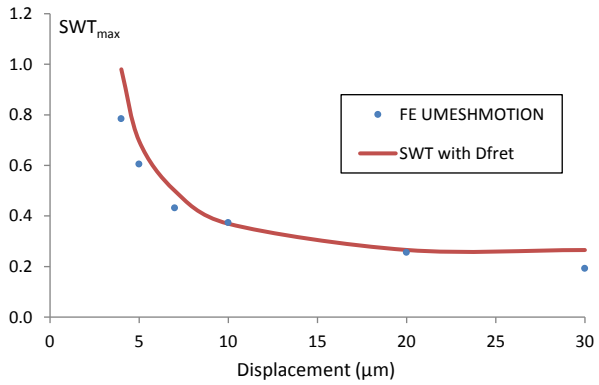

Figure 17. Comparison of effect of displacement on wear simulation SWT_{max} and maximum SWT-D_{fret} value.

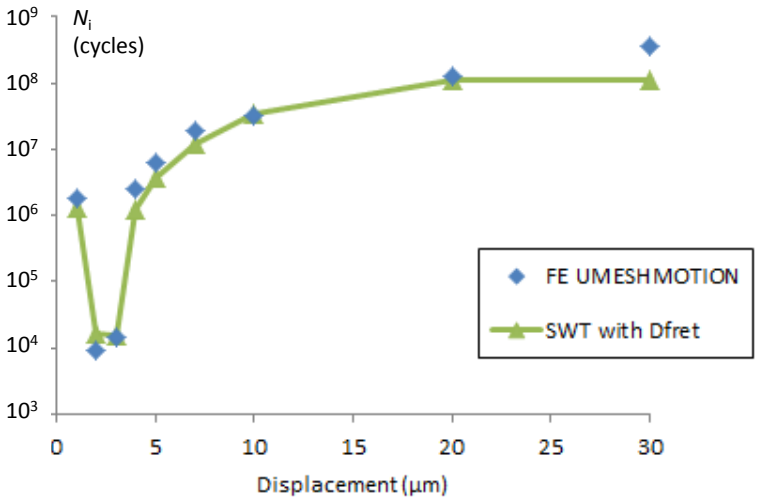

Figure 18. Comparison of effect of displacement on fretting crack initiation life calculated using wear simulated SWT and modified SWT-D_{fret} parameter.

Tables

Table 1. Chemical composition of EN8 steel (from data sheet).

Element	Fe	C	Mg	Si	P	S
Weight (%)	Balance	0.36-0.44	0.60-1.00	0.10-0.40	0.050 Max	0.050 Max

Table 2. Geometry and loading conditions on cylinder-on-flat on fretting test.

Normal load (N)	Stroke (μm)	Frequency (Hz)	Number of fretting cycles
250	15, 30, 50	20	1×10^5
500	15, 30, 50	20	1×10^5

Table 3. Identified low- and high-cycle fatigue constants for pressure amour wire, for crack initiation and failure.

Parameter	Initiation	Failure
σ'_f	1633 MPa	1710 MPa
ε'_f	0.11225	0.2355
b	-0.1118	-0.12
c	-0.5221	-0.5742

Table 4. D_{fret} constants for pressure armour wire.

Parameter	Value
$(\tau\delta)_{th}$	0.4 MPa mm
C	0.05 MPa^{-1} mm^{-1}
m	-0.85